

---

# Kronecker-factored Quasi-Newton Methods for Convolutional Neural Networks

---

Yi Ren<sup>1</sup> Donald Goldfarb<sup>1</sup>

## Abstract

Second-order methods have the capability of accelerating optimization by using much richer curvature information than first-order methods. However, most are impractical in a deep learning setting where the number of training parameters is huge. In this paper, we propose KF-QN-CNN, a new Kronecker-factored quasi-Newton method for training convolutional neural networks (CNNs), where the Hessian is approximated by a layer-wise block diagonal matrix and each layer's diagonal block is further approximated by a Kronecker product corresponding to the structure of the Hessian restricted to that layer. New damping and Hessian-action techniques for BFGS are designed to deal with the non-convexity and the particularly large size of Kronecker matrices in CNN models and convergence results are proved for a variant of KF-QN-CNN under relatively mild conditions. KF-QN-CNN has memory requirements comparable to first-order methods and much less per-iteration time complexity than traditional second-order methods. Compared with state-of-the-art first- and second-order methods on several CNN models, KF-QN-CNN consistently exhibited superior performance in all of our tests.

## 1. Introduction

First-order methods, including stochastic gradient descent (SGD) (Robbins & Monro, 1951) and the class of adaptive learning rate methods such as AdaGrad (Duchi et al., 2011), RMSprop (Hinton et al., 2012), and Adam (Kingma & Ba, 2014), are currently the most popular methods for training deep learning models, such as multilayer perceptrons (MLPs) and convolutional neural networks (CNNs). Although these methods are fairly easy to implement, they use at most, a very limited amount of curvature information to

facilitate optimization. Vanilla SGD uses no curvature information, while the adaptive learning rate methods use a diagonal pre-conditioning matrix based on the second moment of the gradient. As a result, first-order methods can suffer from slow convergence, especially if hyper-parameters are set poorly.

On the other hand, second-order methods use the rich curvature information of the problem to accelerate optimization. Beside the classical Newton method, sub-sampled Newton methods have been proposed to handle large data sets (see e.g., (Xu et al., 2019)), but when the number of training parameters is huge, inverting the Hessian matrix is impractical. Quasi-Newton (QN) methods, ranging from the original BFGS (Broyden, 1970; Fletcher, 1970; Goldfarb, 1970; Shanno, 1970) and limited-memory BFGS (L-BFGS) (Liu & Nocedal, 1989), to more recent developments that take into account stochasticity and/or non-convexity (Byrd et al., 2016; Gower et al., 2016; Wang et al., 2017), avoid the expensive inversion operation. Other methods use surrogates to the Hessian, such as the Gauss-Newton (GN) and Fisher matrices (e.g. natural gradient (NG) method (Amari et al., 2000), Hessian-free method (Martens, 2010), Krylov subspace method (Vinyals & Povey, 2012), sub-sampled GN and NG methods (Ren & Goldfarb, 2019), etc). However, in all of the above-mentioned second-order methods, whether they use the Hessian or a surrogate, the size of the matrix becomes prohibitive when the number of training parameters is huge.

Besides traditional second-order methods, there are special variants of these, which focus on using the Kronecker-factored structure of the deep learning models to reduce their memory and computational requirement. One of the most popular methods of this type is KFAC, which was originally proposed for MLPs (Martens & Grosse, 2015), and later extended to CNNs (Grosse & Martens, 2016). KFAC is a NG method, where the Fisher matrix is approximated by a block-diagonal matrix, each block of which is further approximated by a Kronecker product. Other Kronecker-factored NG methods have also been proposed in (Heskes, 2000; Povey et al., 2014; George et al., 2018). The approximate generalized GN method KFRA (Botev et al., 2017) adopts a block-diagonal Kronecker-factored approximation to the GN matrix for MLPs and computes the diagonal block

<sup>1</sup>Department of Industrial Engineering and Operations Research, Columbia University, USA. Correspondence to: Yi Ren <yr2322@columbia.edu>.

approximations recursively. Lastly, Shampoo (Gupta et al., 2018) extends adaptive learning rate methods by using a block-diagonal Kronecker-factored pre-conditioning matrix. A Kronecker-factored QN method (Goldfarb et al., 2020) for MLPs has also been proposed, and is very closely related to the method proposed in this paper.

### 1.1. Our Contributions

In this paper, we propose KF-QN-CNN, a new class of Kronecker-factored quasi-Newton methods for training CNNs. We first show that for a convolutional layer and a single data-point, the gradient and Hessian restricted to that layer can be approximated by the Kronecker product of two matrices (vectors). We then introduce a class of Kronecker-factored QN methods for CNNs, which are more scalable than classical QN methods. To achieve this, we first adopt a block-diagonal approximation to the Hessian matrix, where each diagonal block corresponds to a layer of the model, and then approximate each such block by a Kronecker product of two matrices so that the inverse Hessian is also approximated by a Kronecker product. We then use BFGS and/or L-BFGS to approximate the inverses, and propose a new damping technique and Hessian-action technique specifically designed for convolutional layers.

Our proposed method KF-QN-CNN has comparable memory requirements to those of first-order methods, while its per-iteration time complexity is smaller, and in many cases, much smaller than that of popular second-order methods (e.g. KFAC) for training CNNs. Further, we prove convergence results for a variant of KF-QN-CNN under relatively mild conditions. In numerical experiments on well-established CNN models, KF-QN-CNN consistently outperformed state-of-the-art first-order (SGD and Adam) and second-order (KFAC) methods.

## 2. Convolutional Layer and its Kronecker-factored Structures

In this section, after first describing the computations involved in CNNs, we reveal the Kronecker structures of the gradient and Hessian of the loss function with respect to a convolutional layer’s parameters for a single data-point. We then extend the Kronecker structure to the case of multiple data-points, which serves as the foundation for our KF-QN-CNN method.

### 2.1. Convolutional Neural Networks

We consider a CNN with  $L$  layers (for simplicity, assume they are all convolutional layers), with trainable parameters consisting of a tensor of weights  $w_l$  and a vector of biases  $b_l$  for  $l \in \{1, \dots, L\}$  and a loss function  $\mathcal{L}$ . For a data-point  $(x, y)$ ,  $x$  is fed into the CNN as input, yielding  $\hat{y}$  as the

output. Note that, the loss  $\mathcal{L}(\hat{y}, y)$  between the output  $\hat{y}$  and  $y$  is a non-convex function of the set of all trainable parameters  $\theta := \{w_1, b_1, \dots, w_L, b_L\}$ .

For a dataset that contains multiple data-points indexed by  $n = 1, \dots, N$ , let  $f(n; \theta)$  denote the loss from the  $n$ th data-point. Thus, viewing the dataset as an empirical distribution, the actual loss function that we wish to minimize is

$$f(\theta) := \mathbb{E}_n[f(n; \theta)] := \frac{1}{N} \sum_{n=1}^N f(n; \theta).$$

Let us now focus on a single convolutional layer from the CNN, and omit the layer index  $l$  for simplicity. A typical convolutional layer consists of the trainable part with trainable parameters (i.e. weights  $w$  and biases  $b$ ) and the non-trainable part (i.e. activation). We focus on the trainable part, since we are primarily interested in optimizing the parameters. For simplicity, we assume that:

1. the convolutional layer is 2-dimensional;
2. the filters are of size  $(2R + 1) \times (2R + 1)$ , with spatial offsets from the centers of each filter indexed by  $\delta \in \Delta := \{-R, \dots, R\} \times \{-R, \dots, R\}$ ;
3. the stride is of length 1, and the padding is equal to  $R$ , so that the sets of input and output spatial locations ( $t \in \mathcal{T} \subset \mathbf{R}^2$ ) are the same.<sup>1</sup>;
4. the layer has  $J$  input channels indexed by  $j = 1, \dots, J$ ,  $I$  output channels indexed by  $i = 1, \dots, I$ .

The weights  $w$ , which correspond to the elements of all of the filters in this layer, can be viewed as a 4-dimensional tensor. Hence, an element of  $w$  is denoted as  $w_{i,j,\delta}$ , where the first two indices  $i, j$  are the output/input channels, and the last two indices  $\delta$  are the spatial offset within a filter. The bias  $b$  is a length- $I$  vector.

Let  $a$ , with components  $a_{j,t}$ , denote the input to the layer after padding is added, where  $t$  denotes the spatial location of the padded input and  $j = 1, \dots, J$ ; and let  $h$ , with components  $h_{i,t}$ , denote the pre-activation output of the layer, where  $t$  denote the spatial location of the output and  $i = 1, \dots, I$ . Given  $a$ ,  $h$  is computed as

$$h_{i,t} = \sum_{j=1}^J \sum_{\delta \in \Delta} w_{i,j,\delta} a_{j,t+\delta} + b_i, \quad t \in \mathcal{T}, i = 1, \dots, I. \quad (1)$$

### 2.2. Single Data-point: Gradient and Hessian Approximations

We now consider a single data-point, omitting the index  $n$  for simplicity, and derive the structure of gradient and Hessian of the function  $f(\cdot; \theta)$ .

<sup>1</sup>The derivations in this paper can also be extended to the case where stride is greater than 1.

We define  $\mathcal{D}X := \frac{\partial f}{\partial X}$  for any variable  $X$  and  $\text{vec}(\cdot)$  to be the vectorization of a matrix. For the pre-activation output and input to the layer, we define, respectively, the vectors

$$\mathbf{h}_t := (h_{1,t}, \dots, h_{I,t})^\top \in \mathbb{R}^I,$$

$$\mathbf{a}_t := (a_{1,t+\delta_1}, \dots, a_{J,t+\delta_{|\Delta|}}, 1)^\top \in \mathbb{R}^{J|\Delta|+1},$$

for  $t \in \mathcal{T}$ . Note that a homogeneous coordinate is concatenated at the end of  $\mathbf{a}_t$ . Also, we use  $\bar{X}$  to denote the value of  $X_t$  averaged over the spatial locations  $\mathcal{T}$  for any quantity  $X$ . Thus,  $\bar{\mathbf{a}} := \frac{1}{|\mathcal{T}|} \sum_{t \in \mathcal{T}} \mathbf{a}_t$ ,  $\bar{\mathbf{h}} := \frac{1}{|\mathcal{T}|} \sum_{t \in \mathcal{T}} \mathbf{h}_t$ . For  $t, t' \in \mathcal{T}$ , we also define the two matrices

$$\begin{aligned} A_{t,t'} &:= \mathbf{a}_t \mathbf{a}_{t'}^\top \in \mathbb{R}^{(J|\Delta|+1) \times (J|\Delta|+1)}, \\ G_{t,t'} &:= \frac{\partial^2 f}{\partial \mathbf{h}_t \partial \mathbf{h}_{t'}} \in \mathbb{R}^{I \times I}. \end{aligned} \quad (2)$$

For the weights and biases, we define the vectors

$$\mathbf{w}_i := (w_{i,1,\delta_1}, \dots, w_{i,J,\delta_{|\Delta|}}, b_i)^\top \in \mathbb{R}^{J|\Delta|+1},$$

for  $i = 1, \dots, I$ , and from them the matrix

$$W := (\mathbf{w}_1, \dots, \mathbf{w}_I)^\top \in \mathbb{R}^{I \times (J|\Delta|+1)}.$$

We first derive the structure of the gradient. By (1),

$$\begin{aligned} \frac{\partial f}{\partial w_{i,j,\delta}} &= \sum_{t \in \mathcal{T}} \frac{\partial f}{\partial h_{i,t}} \frac{\partial h_{i,t}}{\partial w_{i,j,\delta}} = \sum_{t \in \mathcal{T}} \mathcal{D}h_{i,t} a_{j,t+\delta}, \\ \frac{\partial f}{\partial b_i} &= \sum_{t \in \mathcal{T}} \frac{\partial f}{\partial h_{i,t}} \frac{\partial h_{i,t}}{\partial b_i} = \sum_{t \in \mathcal{T}} \mathcal{D}h_{i,t}. \end{aligned}$$

Hence,

$$\mathcal{D}\mathbf{w}_i = \sum_{t \in \mathcal{T}} \mathcal{D}h_{i,t} \mathbf{a}_t \Rightarrow \mathcal{D}W = \sum_{t \in \mathcal{T}} \mathcal{D}\mathbf{h}_t (\mathbf{a}_t)^\top.$$

and  $\text{vec}(\mathcal{D}W) = \sum_{t \in \mathcal{T}} \mathbf{a}_t \otimes \mathcal{D}\mathbf{h}_t$  is the sum of  $|\mathcal{T}|$  Kronecker products.

To derive the Hessian of  $f(\cdot; \theta)$  for a single data-point, it follows from (1) that

$$\begin{aligned} \frac{\partial(\mathcal{D}h_{i,t})}{\partial w_{i',j,\delta}} &= \sum_{t'} \frac{\partial(\mathcal{D}h_{i,t})}{\partial h_{i',t'}} \frac{\partial h_{i',t'}}{\partial w_{i',j,\delta}} = \sum_{t'} \frac{\partial^2 f}{\partial h_{i,t} \partial h_{i',t'}} a_{j,t'+\delta}, \\ \frac{\partial(\mathcal{D}h_{i,t})}{\partial b_{i'}} &= \sum_{t'} \frac{\partial(\mathcal{D}h_{i,t})}{\partial h_{i',t'}} \frac{\partial h_{i',t'}}{\partial b_{i'}} = \sum_{t'} \frac{\partial^2 f}{\partial h_{i,t} \partial h_{i',t'}}. \end{aligned}$$

Hence,

$$\frac{\partial(\mathcal{D}h_{i,t})}{\partial \mathbf{w}_{i'}} = \sum_{t'} \frac{\partial^2 f}{\partial h_{i,t} \partial h_{i',t'}} \mathbf{a}_{t'},$$

and

$$\begin{aligned} \frac{\partial^2 f}{\partial \mathbf{w}_i \partial \mathbf{w}_{i'}} &= \frac{\partial}{\partial \mathbf{w}_{i'}} \left( \sum_t \mathcal{D}h_{i,t} \mathbf{a}_t \right) \\ &= \sum_t \frac{\partial(\mathcal{D}h_{i,t})}{\partial \mathbf{w}_{i'}} \mathbf{a}_t^\top = \sum_t \sum_{t'} \frac{\partial^2 f}{\partial h_{i,t} \partial h_{i',t'}} A_{t,t'}. \end{aligned}$$

Hence,

$$\frac{\partial^2 f}{\partial \text{vec}(W)^2} = \sum_{t,t'} A_{t,t'} \otimes G_{t,t'}.$$

If we **assume** that  $G_{t,t'} = 0$  for any  $t \neq t'$ , we have that

$$\frac{\partial^2 f}{\partial \text{vec}(W)^2} \approx \sum_{t \in \mathcal{T}} A_{t,t} \otimes G_{t,t}. \quad (3)$$

As in other methods that have been proposed for training deep learning models that use Kronecker factored approximations to Hessian or other preconditioning matrices (Grosse & Martens, 2016; Botev et al., 2017; Goldfarb et al., 2020), we further approximate  $\frac{\partial^2 f}{\partial \text{vec}(W)^2}$  by a single Kronecker product. To achieve this, we now approximate the average of the Kronecker products of a set of matrix pairs  $\{(U_t, V_t)\}$  by the Kronecker product of the averages of individual sets of matrices  $\{U_t\}$ ,  $\{V_t\}$ , i.e.,

$$\frac{1}{|\mathcal{T}|} \sum_{t \in \mathcal{T}} U_t \otimes V_t \approx \left( \frac{1}{|\mathcal{T}|} \sum_{t \in \mathcal{T}} U_t \right) \otimes \left( \frac{1}{|\mathcal{T}|} \sum_{t \in \mathcal{T}} V_t \right). \quad (4)$$

Applying (4) to (3), we have that

$$\begin{aligned} \frac{\partial^2 f}{\partial \text{vec}(W)^2} &\approx |\mathcal{T}| \cdot \left( \frac{1}{|\mathcal{T}|} \sum_{t \in \mathcal{T}} A_{t,t} \right) \otimes \left( \frac{1}{|\mathcal{T}|} \sum_{t \in \mathcal{T}} G_{t,t} \right) \\ &= \left( \sum_{t \in \mathcal{T}} A_{t,t} \right) \otimes \left( \frac{1}{|\mathcal{T}|} \sum_{t \in \mathcal{T}} G_{t,t} \right). \end{aligned} \quad (5)$$

Note that the assumptions that we made in this subsection are analogous to the IAD (Independent Activations and Derivatives), SH (Spatial Homogeneity), and SUD (Spatially Uncorrelated Derivatives) assumptions in (Grosse & Martens, 2016).

### 2.3. Further Approximation for Multiple Data-points

In the case of multiple data-points, we use  $(n)$  to denote the index of a data point. To approximate the average Hessian across multiple data-points as a single Kronecker product, we again use (4), but this time averaging over the data points.

By (5), we have that

$$\begin{aligned} \frac{\partial^2 f}{\partial \text{vec}(W)^2} &= \mathbb{E}_n \left[ \frac{\partial^2 f(n)}{\partial \text{vec}(W)^2} \right] \\ &\approx \mathbb{E}_n \left[ \left( \sum_{t \in \mathcal{T}} A_{t,t}(n) \right) \otimes \left( \frac{1}{|\mathcal{T}|} \sum_{t \in \mathcal{T}} G_{t,t}(n) \right) \right] \end{aligned} \quad (6)$$

$$\approx A \otimes G, \quad (7)$$

where

$$A := \mathbb{E}_n \left[ \sum_{t \in \mathcal{T}} A_{t,t}(n) \right], G := \mathbb{E}_n \left[ \frac{1}{|\mathcal{T}|} \sum_{t \in \mathcal{T}} G_{t,t}(n) \right]. \quad (8)$$

### 3. KF-QN-CNN Method

In order to obtain an efficient quasi-Newton method for CNNs, we first approximate the Hessian of  $f(\theta)$  by a block diagonal matrix, where each block corresponds to the Hessian with respect to a layer. As a result, the parameters of each layer can be updated separately.

For a single convolutional layer, let  $H_A$  and  $H_G$  be approximations to  $A^{-1}$  and  $G^{-1}$ , respectively. By (7),  $\left( \frac{\partial^2 f}{\partial \text{vec}(W)^2} \right)^{-1}$  can be approximate by  $H_A \otimes H_G$ , and we can update the parameters of this layer by computing

$$W^+ = W - \alpha H_G (DW) H_A,$$

where  $\alpha$  denotes the learning rate. In the following two subsections, we describe how to apply BFGS updating to approximate  $H_A$  and  $H_G$  for a single convolutional layer.

#### 3.1. QN Approximation for $G^{-1}$

Given an approximation  $H$  to the inverse of a symmetric matrix  $B$ , the BFGS updating formula computes

$$H^+ = (I - \rho \mathbf{s} \mathbf{y}^\top) H (I - \rho \mathbf{y} \mathbf{s}^\top) + \rho \mathbf{s} \mathbf{s}^\top, \quad (9)$$

with given vectors  $\mathbf{s}, \mathbf{y}$  ( $\mathbf{y} \approx B\mathbf{s}$ ) and  $\rho = \frac{1}{\mathbf{y}^\top \mathbf{s}}$ . Clearly, the updated approximating matrix  $H^+$  satisfies the so-called secant condition  $H^+ \mathbf{y} = \mathbf{s}$ .

In the case of a single data-point, recall that  $B = G_{t,t}(n) = \frac{\partial^2 f(n)}{\partial \mathbf{h}_t(n)^2}$ , for a given  $t$ . Hence,  $(\mathbf{s}, \mathbf{y}) = (\mathbf{h}_t^+(n) - \mathbf{h}_t(n), \mathcal{D}\mathbf{h}_t^+(n) - \mathcal{D}\mathbf{h}_t(n))$ . To approximate  $B = \frac{1}{|\mathcal{T}|} \sum_{t \in \mathcal{T}} G_{t,t}(n)$ , we average the  $(\mathbf{s}, \mathbf{y})$  pairs across  $\mathcal{T}$ , resulting in  $(\mathbf{s}, \mathbf{y}) = (\overline{\mathbf{h}^+}(n) - \overline{\mathbf{h}}(n), \overline{\mathcal{D}\mathbf{h}^+}(n) - \overline{\mathcal{D}\mathbf{h}}(n))$ . Finally, to approximate  $G$  in (8), which is an average across multiple data-points,  $(\mathbf{s}, \mathbf{y}) = (\mathbf{s}_G, \mathbf{y}_G)$ , where

$$\mathbf{s}_G = \mathbb{E}_n \left[ \overline{\mathbf{h}^+}(n) - \overline{\mathbf{h}}(n) \right], \quad (10)$$

$$\mathbf{y}_G = \mathbb{E}_n \left[ \overline{\mathcal{D}\mathbf{h}^+}(n) - \overline{\mathcal{D}\mathbf{h}}(n) \right]. \quad (11)$$

**Algorithm 1**  $D_P D_{LM}$ : a new double damping procedure

---

```

1: Input:  $\mathbf{s}, \mathbf{y}$ ; Output:  $\tilde{\mathbf{s}}, \tilde{\mathbf{y}}$ ; Given:  $H, 0 < \mu_1 < 1,$ 
    $\mu_2 > 0$ 
2: if  $\mathbf{s}^\top \mathbf{y} < \mu_1 \mathbf{y}^\top H \mathbf{y}$  then
3:    $\theta_1 = \frac{(1-\mu_1) \mathbf{y}^\top H \mathbf{y}}{\mathbf{y}^\top H \mathbf{y} - \mathbf{s}^\top \mathbf{y}}$ 
4: else
5:    $\theta_1 = 1$ 
6: end if
7:  $\tilde{\mathbf{s}} = \theta_1 \mathbf{s} + (1 - \theta_1) H \mathbf{y}$  {Powell's damping on  $H$ }
8:  $\tilde{\mathbf{y}} = \mathbf{y} + \mu_2 \tilde{\mathbf{s}}$  {Levenberg-Marquardt damping on  $H^{-1}$ }
9: return:  $\tilde{\mathbf{s}}, \tilde{\mathbf{y}}$ 

```

---

Because of the non-convex nature of the CNN model, there is no guarantee that  $G$  is positive definite. Hence, it is possible that  $\mathbf{s}^\top \mathbf{y} < 0$ . Moreover, if the expectation is estimated over a mini-batch,  $(\mathbf{s}, \mathbf{y})$  will exhibit a certain amount of stochasticity. To deal with these concerns, we propose a double damping (DD) procedure  $D_P D_{LM}$  in Algorithm 1, where  $P$  stands for Powell's damping and  $LM$  stands for Levenberg-Marquardt (LM) damping.

Note that in the DD procedure proposed in (Goldfarb et al., 2020), the parameter  $\mu_2$  can only take values in  $(0, 1]$ . However, in  $D_P D_{LM}$ , the parameter  $\mu_2$  can take values in  $(0, \infty)$  and is more naturally related to LM damping. To see this connection, note that in Algorithm 1, after Powell's damping on  $H$ ,  $\tilde{\mathbf{s}}^\top \mathbf{y} \geq \mu_1 \mathbf{y}^\top H \mathbf{y} \geq 0$ . Hence,  $\tilde{\mathbf{s}}^\top \tilde{\mathbf{y}} \geq \mu_2 \|\tilde{\mathbf{s}}\|^2$ , which can be viewed as LM damping with a parameter of  $\mu_2$ , since  $G$  is then lower bounded by  $\mu_2 I$ .

#### 3.2. QN Approximation for $A^{-1}$

To estimate the inverse of  $A$ , we use the Hessian-action BFGS updating technique proposed in (Goldfarb et al., 2020), with several modifications for convolutional layers. Given the current estimate  $H_A$  of  $A^{-1}$ , the  $(\mathbf{s}, \mathbf{y})$  pair for updating  $H_A$  are computed as:

$$\mathbf{s}_A = H_A \hat{\mathbf{a}}, \quad \mathbf{y}_A = A \mathbf{s}_A + \lambda_A \mathbf{s}_A, \quad (12)$$

where  $\hat{\mathbf{a}} = \mathbb{E}_n \left[ \frac{1}{|\mathcal{T}|} \sum_{t \in \mathcal{T}} \mathbf{a}_t(n) \right]$  and  $\lambda_A$  is the damping value. The differences from the technique in (Goldfarb et al., 2020) are:

- We do not use moving average to estimate  $A$ . Instead, we estimate it from the current mini-batch. As a result, no decay parameter is needed.
- Since  $A$  is estimated from a mini-batch, we compute  $A \mathbf{s}_A$  without explicitly computing  $A$ . To be specific,

by (2) and (8),

$$\begin{aligned} As_A &= \mathbb{E}_n \left[ \sum_{t \in \mathcal{T}} \mathbf{a}_t(n) \mathbf{a}_t(n)^\top \right] s_A \\ &= \mathbb{E}_n \left[ \sum_{t \in \mathcal{T}} (\mathbf{a}_t(n)^\top s_A) \mathbf{a}_t(n) \right]. \end{aligned} \quad (13)$$

- $s_A$  is slightly different from the  $s_A$  in (Goldfarb et al., 2020): For a fully-connected layer,  $A$  is the average of multiple symmetric outer products of  $\mathbf{a}$ 's and  $s_A$  involves the  $\mathbf{a}$  vector averaged across multiple data-points. On the other hand, for a convolutional layer,  $A$  is the average of multiple outer products over both spatial location  $\mathcal{T}$  and multiple data-points. Thus, we start  $s_A$  with the  $\mathbf{a}$  vector averaged across both  $\mathcal{T}$  and multiple data-points, as shown in (12).

### 3.3. Usage of Mini-batches and Moving Averages

Because there is usually a large amount of data, we use mini-batches to estimate the quantities needed for KF-QN-CNN at every iteration. We use  $\bar{X}$  to denote the average value of  $X$  over a minibatch for any quantity  $X$ . Moreover, we use moving averages to both reduce the stochasticity and incorporate more information from the past:

- Gradient. At every iteration, the gradient is estimated from a mini-batch. We also use a moving average scheme to get a better estimate of the gradient, i.e.

$$\widehat{DW} = \beta \widetilde{DW} + (1 - \beta) \widehat{DW}.$$

- BFGS updating for  $H_G$ . By (10) and (11), we use both a mini-batch and moving averages to estimate the  $(s, y)$  for  $H_G$ , i.e.

$$\begin{aligned} s_G &= \beta s_G + (1 - \beta) \left( \widetilde{\mathbf{h}^+} - \widetilde{\mathbf{h}} \right), \\ y_G &= \beta y_G + (1 - \beta) \left( \widetilde{D\mathbf{h}^+} - \widetilde{D\mathbf{h}} \right). \end{aligned}$$

- BFGS updating for  $H_A$ . In (12), we estimate the value of  $A$  from the current minibatch, i.e.  $\sum_{t \in \mathcal{T}} A_{t,t}$ , as well as  $\hat{\mathbf{a}} = \widetilde{\mathbf{a}}$ . Note that  $As_A$  can be computed without forming  $A$ .

### 3.4. Pseudo-code for KF-QN-CNN

Algorithm 2 gives the pseudo-code for KF-QN-CNN. Note that one can use either BFGS or L-BFGS update for  $H_G$ , in which case we name the algorithm KF-BFGS-CNN and KF-BFGS(L)-CNN, respectively. For simplicity, we assume that all layers in the CNN are convolutional layers. Note that KF-QN-CNN can easily be adapted to fully-connected layers, which often constitute the last, or last few, layers of a CNN model.

### Algorithm 2 Pseudo-code for KF-QN-CNN

---

**Require:** Given learning rates  $\{\alpha_k\}$ , damping value  $\lambda$ , batch sizes  $\{m_k\}$

- 1:  $\mu_1 = 0.2, \beta = 0.9; \lambda_A = \lambda_G = \sqrt{\lambda}$
- 2:  $\widehat{DW}_l = 0, A_l = \mathbb{E}_n \left[ \sum_{t \in \mathcal{T}} \mathbf{a}_t^l(n) \mathbf{a}_t^l(n)^\top \right], H_A^l = (A_l + \lambda_A I_A)^{-1}, H_G^l = I, s_G^l = y_G^l = 0 \ (l = 1, \dots, L)$  {Initialization}
- 3: **for**  $k = 1, 2, \dots$  **do**
- 4:   Sample mini-batch  $M_k$  of size  $m_k$
- 5:   Perform a forward-backward pass over  $M_k$  to compute stochastic gradient  $\widetilde{DW}_l \ (l = 1, \dots, L)$
- 6:   **for**  $l = 1, \dots, L$  **do**
- 7:      $\widehat{DW}_l = \beta \widetilde{DW}_l + (1 - \beta) \widehat{DW}_l$
- 8:      $W_l = W_l - \alpha_k H_G^l \widehat{DW}_l H_A^l$  {if L-BFGS is used for  $H_G^l$ , it is initialized as an identity matrix}
- 9:   **end for**
- 10:   Perform another forward-backward pass over  $M_k$  to compute  $\widetilde{\mathbf{h}_l^+}$  and  $\widetilde{D\mathbf{h}_l^+} \ (l = 1, \dots, L)$
- 11:   **for**  $l = 1, \dots, L$  **do**
- 12:     {Update  $H_A^l$  by BFGS}
- 13:      $s_A^l = H_A^l \widetilde{\mathbf{a}_l}, y_A^l = \widetilde{A}_l s_A^l + \lambda_A s_A^l$  using (13)
- 14:     Use BFGS with  $(s_A^l, y_A^l)$  to update  $H_A^l$
- 15:     {Update  $H_G^l$  by damped BFGS or L-BFGS}
- 16:      $s_G^l = \beta s_G^l + (1 - \beta) \left( \widetilde{\mathbf{h}_l^+} - \widetilde{\mathbf{h}_l} \right), y_G^l = \beta y_G^l + (1 - \beta) \left( \widetilde{D\mathbf{h}_l^+} - \widetilde{D\mathbf{h}_l} \right).$
- 17:      $(\widetilde{s}_G^l, \widetilde{y}_G^l) = D_P D_{LM}(s_G^l, y_G^l)$  with  $H = H_G^l, \mu_1 = \mu_1, \mu_2 = \lambda_G$  {See Algorithm 1}
- 18:     Use BFGS or L-BFGS with  $(\widetilde{s}_G^l, \widetilde{y}_G^l)$  to update  $H_G^l$
- 19:   **end for**
- 20: **end for**

---

When using the L-BFGS derived matrix  $H_G^l$  to compute  $H_G^l \widehat{DW}_l$ , instead of using the classical two-loop recursion of L-BFGS, we follow the "non-loop" implementation in (Byrd et al., 1994), which is faster in practice because  $\widehat{DW}_l$  is a matrix, not a vector.

Note that Algorithm 2 contains only one damping hyperparameter (HP)  $\lambda$ , and sets  $\lambda_A = \lambda_G = \sqrt{\lambda}$ . Adding  $\lambda_A s_A^l$  and  $\lambda_G s_G^l$ , respectively, to the vectors  $y_A^l$  and  $y_G^l$  before applying BFGS (or L-BFGS) to  $H_A^l$  and  $H_G^l$ , can be viewed as an approximation to adding the overall LM damping factor  $\lambda I$  to  $(H^l)^{-1} = (H_A^l)^{-1} \otimes (H_G^l)^{-1}$  prior to updating.

## 4. Space and Computational Requirements

In this section, we compare the space and computational requirements of the KF-QN-CNN methods with Adam and



Table 1. Storage

Algorithm	$DW$	$DW \odot DW$	$A$	$G$	Total
KF-BFGS-CNN	$O(IJ \Delta )$	—	$O(J^2 \Delta ^2)$	$O(I^2)$	$O(J^2 \Delta ^2 + IJ \Delta  + I^2)$
KF-BFGS(L)-CNN	$O(IJ \Delta )$	—	$O(J^2 \Delta ^2)$	$O(pI)$	$O(J^2 \Delta ^2 + IJ \Delta  + pI)$
KFAC	$O(IJ \Delta )$	—	$O(J^2 \Delta ^2)$	$O(I^2)$	$O(J^2 \Delta ^2 + IJ \Delta  + I^2)$
Adam	$O(IJ \Delta )$	$O(IJ \Delta )$	—	—	$O(IJ \Delta )$

Table 2. Computation per iteration beyond that required for the mini-batch stochastic gradient

Algorithm	Additional pass	Curvature	Step $\Delta W_l$
KF-BFGS-CNN	$O(mIJ \Delta  \mathcal{T} )$	$O(mJ \Delta  \mathcal{T}  + J^2 \Delta ^2 + mI \mathcal{T}  + I^2)$	$O(IJ^2 \Delta ^2 + I^2J \Delta )$
KF-BFGS(L)-CNN	$O(mIJ \Delta  \mathcal{T} )$	$O(mJ \Delta  \mathcal{T}  + J^2 \Delta ^2 + mI \mathcal{T}  + pI)$	$O(IJ^2 \Delta ^2 + pIJ \Delta )$
KFAC	$O(mIJ \Delta  \mathcal{T} )$	$O(m(J^2 \Delta ^2 + I^2) \mathcal{T}  + \frac{1}{T}(J^3 \Delta ^3 + I^3))$	$O(IJ^2 \Delta ^2 + I^2J \Delta )$
Adam	—	$O(IJ \Delta )$	$O(IJ \Delta )$

KFAC, which are among the predominant first and second order methods, respectively, used to train CNNs.

We focus on one convolutional layer, with  $J$  input channels,  $I$  output channels, kernel size  $|\Delta|$ , and  $|\mathcal{T}|$  spacial locations. Moreover, let  $m$  denote the size of mini-batch,  $p$  denote the number of  $(\mathbf{s}, \mathbf{y})$  pairs for L-BFGS, and  $T$  denote the frequency of matrix inversion for KFAC.

From Table 1, one can see that KF-QN-CNN requires roughly the same amount of memory as KFAC. Note that  $I$  and  $J$  are usually much larger than  $|\Delta|$  in CNNs. For example, in VGG16 (Simonyan & Zisserman, 2014),  $I$  and  $J$  can be as large as 512 whereas  $|\Delta| = 9$ . Hence, as Table 1 shows, the memory required by KF-QN-CNN is of the same order as that of Adam in terms of  $I$  and  $J$ .

In Table 2, besides the operations listed, each algorithm also needs to compute the mini-batch gradient requiring  $O(mIJ|\Delta||\mathcal{T}|)$  time. (Note that  $|\mathcal{T}|$  is usually much larger than  $I$  or  $J$ .) KF-QN-CNN requires considerably less time to compute curvature information than KFAC. First, KF-QN-CNN avoids matrix inversion, whose complexity is cubic in  $I$  and  $J|\Delta|$  (although this is amortized in KFAC by  $\frac{1}{T}$  by using the same inverse for  $T$  iterations). Second, KF-QN-CNN avoids computing the  $\Omega$  and  $\Gamma$  matrices of KFAC from mini-batch data, whose complexity is  $m(J^2|\Delta|^2 + I^2)|\mathcal{T}|$ . Instead, we directly compute the  $(\mathbf{s}, \mathbf{y})$  pairs for  $H_A$  and  $H_G$ , without explicitly forming  $A$  or  $G$ . Compared with Adam, the computational time required by KF-QN-CNN typically is larger by a factor that is less than 4 (e.g., see the numerical results in Section 6 and the Appendix).

## 5. Convergence Results

In this section, following the framework in (Wang et al., 2017), we present convergence results for Algorithm 3, a variant of KF-BFGS(L)-CNN (see the Appendix). For the

purpose of simplicity, we assume that all layers are convolutional. (Note that our results still hold if there are some fully-connected layers in the model.)

Algorithm 3 differs from the actual implementation as specified in Algorithm 2, in that the gradient is estimated from the current minibatch without momentum, and  $H_A^l$  is computed by simply inverting  $A_l + \lambda_A I$ , instead of using Hessian-action BFGS. Moreover, in Algorithm 3,  $D_{P(I)}D_{LM}$  (see Algorithm 4 in the appendix) is used instead of  $D_P D_{LM}$  (Algorithm 1).  $D_{P(I)}D_{LM}$  differs from  $D_P D_{LM}$  by replacing  $H$  by the identity matrix  $I$ , where it appears in Algorithm 1. This is justifiable partly because, in our actual implementation of L-BFGS,  $H_G$  is always initialized with an identity matrix. By using  $D_{P(I)}D_{LM}$ , we have

**Lemma 1.** *The output of  $D_{P(I)}D_{LM}$  satisfies:  $\frac{\tilde{\mathbf{s}}^\top \tilde{\mathbf{s}}}{\tilde{\mathbf{s}}^\top \tilde{\mathbf{y}}} \leq \frac{1}{\mu_2}$ ,  $\frac{\tilde{\mathbf{y}}^\top \tilde{\mathbf{y}}}{\tilde{\mathbf{s}}^\top \tilde{\mathbf{y}}} \leq \frac{1}{\mu_3}$ , where  $\mu_3 = \frac{\mu_1}{1+2\mu_1\mu_2}$ .*

Consequently, one can prove the following two lemmas:

**Lemma 2.** *Suppose that we use  $(\mathbf{s}, \mathbf{y})$  for the BFGS update (9). If  $\frac{\mathbf{s}^\top \mathbf{s}}{\mathbf{s}^\top \mathbf{y}} \leq \frac{1}{\mu_2}$ ,  $\frac{\mathbf{y}^\top \mathbf{y}}{\mathbf{s}^\top \mathbf{y}} \leq \frac{1}{\mu_3}$ , then  $\|B^+\| \leq \|B\| + \frac{1}{\mu_3}$  and  $\|H^+\| \leq (1 + \frac{1}{\sqrt{\mu_2\mu_3}})^2 \|H\| + \frac{1}{\mu_2}$ , where  $B$  denotes the inverse of  $H$ .*

**Lemma 3.** *For Algorithm 3, there exist two positive constants  $\underline{\kappa}_G$  and  $\bar{\kappa}_G$ , such that  $\underline{\kappa}_G I \preceq H_G^l(k) \preceq \bar{\kappa}_G I, \forall k, l$ .*

To apply the convergence results in (Wang et al., 2017) to Algorithm 3, we need to have that  $H_A^l$ , and hence that  $H_l = H_A^l \otimes H_G^l$  is bounded above and below by positive definite matrices, in addition to  $H_G^l$ . For this purpose and for satisfying other requirements needed to apply the theory in (Wang et al., 2017), we make the following assumptions:

**AS. 1.**  $f: \mathbb{R}^d \rightarrow \mathbb{R}$  is continuously differentiable.  $f(\theta)$  is lower bounded by a real number  $f^{\text{low}}$  for any  $\theta \in \mathbb{R}^d$ .  $\nabla f$  is globally Lipschitz continuous with Lipschitz constant  $L$ ,

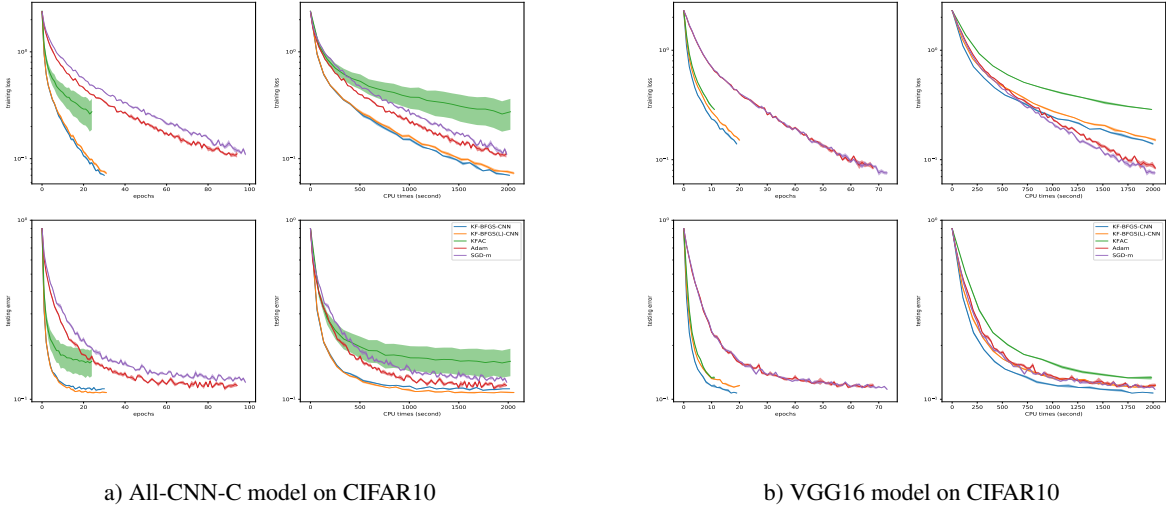


Figure 1. Comparison between algorithms on CIFAR10 with two CNN models

i.e. for any  $\theta, \theta' \in \mathbb{R}^d$ ,  $\|\nabla f(\theta) - \nabla f(\theta')\| \leq L\|\theta - \theta'\|$ .

**AS. 2.** For every iteration  $k$ , we have

$$\begin{aligned} a) \mathbb{E}_{\xi_k} [g(\theta_k, \xi_k)] &= \nabla f(\theta_k), \\ b) \mathbb{E}_{\xi_k} [\|g(x_k, \xi_k) - \nabla f(\theta_k)\|^2] &\leq \sigma^2, \end{aligned}$$

where  $g$  is the minibatch gradient and  $\sigma > 0$  is the noise level of the gradient estimation, and  $\xi_k, k = 1, 2, \dots$  are independent samples, and for a given  $k$  the random variable  $\xi_k$  is independent of  $\{\theta_j\}_{j=1}^k$

**AS. 3.** The inputs  $a_{j,t}^l$ 's to any layers are bounded, i.e.  $\exists \varphi > 0$  s.t.  $\forall l, j, t, |a_{j,t}^l| \leq \varphi$ .

Note that AS. 3 is relatively mild, in the sense that it is fulfilled if the activation functions of the model are all bounded (e.g. sigmoid, tanh, binary step), or some kind of "normalization" is performed before the data are fed into each layer.

We now show that our block-diagonal approximation to Hessian is bounded below and above by positive definite matrices in Lemma 4, and after that, applying Theorem 2.8 in (Wang et al., 2017) we obtain our main convergence result, Theorem 1. The complete proofs of all of the lemmas and the theorem in this section are deferred to Sec A.1 in the appendix.

**Lemma 4.** For Algorithm 3, under the assumption AS. 3, (i)  $\hat{A}_l \preceq (J|\Delta|\varphi^2 + 1)|\mathcal{T}|I$ , and (ii) there exist two positive constants  $\underline{\kappa}$  and  $\bar{\kappa}$ , such that  $\underline{\kappa}I \preceq H = \text{diag}\{H_1, \dots, H_L\} \preceq \bar{\kappa}I$ .

**Theorem 1.** Suppose that assumptions AS.1, AS.2, AS.3 hold for  $\{\theta_k\}$  generated by Algorithm 3 with batch size  $m_k = m$  for all  $k$ . We also assume that  $\alpha_k$  is specifically

chosen as  $\alpha_k = \frac{\kappa}{L\bar{\kappa}^2}k^{-\beta}$  with  $\beta \in (0.5, 1)$ . Then

$$\begin{aligned} \frac{1}{K} \sum_{k=1}^K \mathbb{E} [\|\nabla f(\theta_k)\|^2] &\leq \frac{2L(M_f - f^{low})\bar{\kappa}^2}{\underline{\kappa}^2} K^{\beta-1} \\ &\quad + \frac{\sigma^2}{(1-\beta)m} (K^{-\beta} - K^{-1}), \end{aligned}$$

where  $K$  denotes the iteration number and  $M_f$  is a positive constant. Moreover, for a given  $\epsilon \in (0, 1)$ , to guarantee that  $\frac{1}{K} \sum_{k=1}^K \mathbb{E} [\|\nabla f(\theta_k)\|^2] < \epsilon$ , the number of iterations  $K$  needed is at most  $O\left(\epsilon^{-\frac{1}{1-\beta}}\right)$ .

Theorem 1 shows that Algorithm 3 converges to a stationary point for a (possibly) non-convex function  $f$ . We note that under very similar assumptions, Theorems 2.5 and 2.6 in (Wang et al., 2017) also hold for Algorithm 3.

## 6. Numerical Results

To demonstrate the performance of KF-QN-CNN, we tested both the BFGS and L-BFGS variants, as well as KFAC, Adam, and SGD-m (i.e. SGD with momentum), on two CNN models that have been found to be effective, namely, All-CNN-C in (Springenberg et al., 2014), and VGG16 in (Simonyan & Zisserman, 2014); (see Sec B.2 in the appendix for more details about the experimental set-up). We experimented on both models, using two datasets, CIFAR-10 (Fig 1) and CIFAR-100 (Fig 2) (Krizhevsky et al., 2009), each of which includes 50,000 training samples and 10,000 testing samples. Minibatches of size 256 were used for all experiments. For both datasets, we applied the data augmentation techniques in (Krizhevsky et al., 2012). Note that the

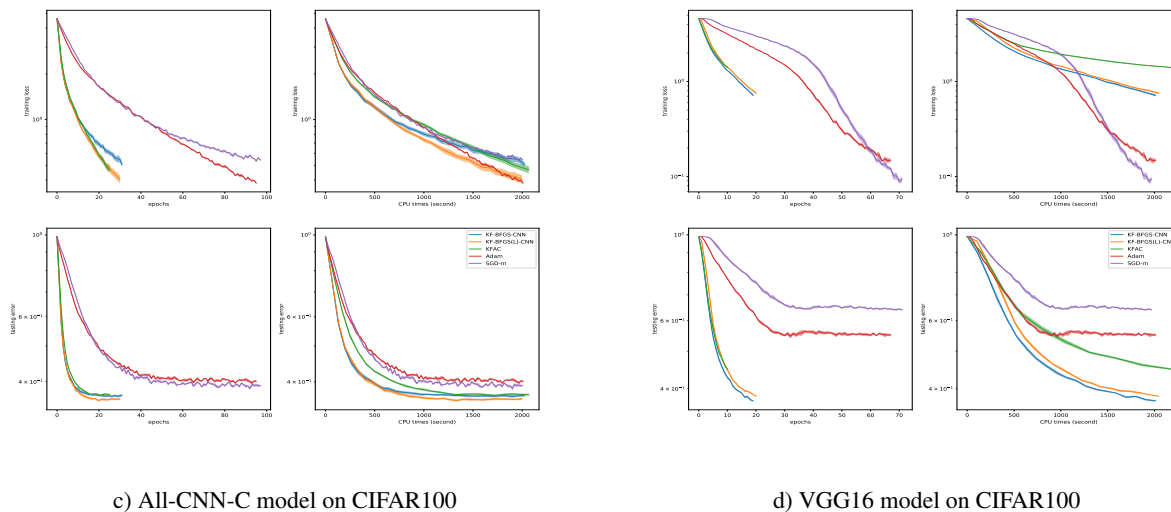


Figure 2. Comparison between algorithms on CIFAR100 with two CNN models

above model/dataset choices have been used and endorsed in many papers, e.g. (Schneider et al., 2019; Choi et al., 2019).

It is common practice to use a decreasing schedule (often chosen heuristically) for the learning rate when training CNNs. Since the primary purpose of our experiments was to compare our algorithms with current state-of-the-art methods for training CNNs, rather than to achieve the best possible results, we chose to use a constant learning rate.

To obtain the results reported in Figures 1 and 2, we first conducted a grid search on the damping and learning rate hyper-parameters (HPs) for all methods (only learning rate for SGD-m). Then, we selected HP values that gave the smallest training loss (the grid search ranges and the best HP values so determined, are listed in Sec B.2 in the appendix). Finally, we ran each algorithm with their best HPs, using 5 different random seeds. The mean values are plotted as solid curves, and  $\pm \text{std}/\sqrt{5}$  for each is depicted as a shaded area<sup>2</sup>.

For each sub-figure in Figures 1 and 2, we report training cross-entropy loss in the upper row and testing classification error in the lower row, and progress with respect to epochs in the left column and CPU time in the right column. All algorithms were run for 2000 CPU seconds.

Figures 1 and 2 show that, in terms of epochs, KF-BFGS-CNN and KF-BFGS(L)-CNN always performed better in our experiments than the other algorithms (or at least as well as the best ones), except for minimizing the training

loss in Figure 2 d), where the first-order methods overfit the training set. Moreover, in terms of generalization, KF-BFGS-CNN and KF-BFGS(L)-CNN outperformed the other algorithms, in all of our tests. Lastly, our methods appeared to be not very sensitive to the choice of HP values (see Sec B.3 in the appendix for more details).

To double-check the over-fitting problem in Fig 2 d), we also tried selecting the best HP values based on testing accuracy (think of it as validation). See Sec B.4 in the appendix, where the results looked similar to those in Figure 1 b).

Finally, it is clear from Figures 1 and 2 that both of our Kronecker-factored QN methods outperformed KFAC in terms of CPU time. We note that our version of KFAC (see Sec B.1 in the Appendix) was not identical to the KFC-pre version developed in (Grosse & Martens, 2016) for training CNNs, which, for example, uses parameter averaging and momentum for adjusting the step direction, and hence is structured like a Kronecker-factored Fisher pre-conditioned SGD method with momentum.

## 7. Conclusion

In this paper, we proposed KF-QN-CNN, a new class of Kronecker-factored quasi-Newton methods for training CNN models, that outperformed state-of-the-art first and second order methods on several CNN problems. We believe that these methods are the first QN methods that are practical for training CNNs. These methods also have the potential for application to more sophisticated models such as ResNet, which include other trainable parameters coming from the batch normalization layers.

<sup>2</sup>Experiments were run on a machine with 8 Intel Xeon E5-2650v4 CPUs with one Nvidia P100 GPU.



## References

- Amari, S.-I., Park, H., and Fukumizu, K. Adaptive method of realizing natural gradient learning for multilayer perceptrons. *Neural computation*, 12(6):1399–1409, 2000.
- Botev, A., Ritter, H., and Barber, D. Practical gauss-newton optimisation for deep learning. In *Proceedings of the 34th International Conference on Machine Learning-Volume 70*, pp. 557–565. JMLR. org, 2017.
- Broyden, C. G. The convergence of a class of double-rank minimization algorithms 1. general considerations. *IMA Journal of Applied Mathematics*, 6(1):76–90, 1970.
- Byrd, R. H., Nocedal, J., and Schnabel, R. B. Representations of quasi-newton matrices and their use in limited memory methods. *Mathematical Programming*, 63(1-3): 129–156, 1994.
- Byrd, R. H., Hansen, S. L., Nocedal, J., and Singer, Y. A stochastic quasi-newton method for large-scale optimization. *SIAM Journal on Optimization*, 26(2):1008–1031, 2016.
- Choi, D., Shallue, C. J., Nado, Z., Lee, J., Maddison, C. J., and Dahl, G. E. On empirical comparisons of optimizers for deep learning. *arXiv preprint arXiv:1910.05446*, 2019.
- Duchi, J., Hazan, E., and Singer, Y. Adaptive subgradient methods for online learning and stochastic optimization. *Journal of Machine Learning Research*, 12(Jul):2121–2159, 2011.
- Fletcher, R. A new approach to variable metric algorithms. *The computer journal*, 13(3):317–322, 1970.
- George, T., Laurent, C., Bouthillier, X., Ballas, N., and Vincent, P. Fast approximate natural gradient descent in a kronecker factored eigenbasis. In *Advances in Neural Information Processing Systems*, pp. 9550–9560, 2018.
- Goldfarb, D. A family of variable-metric methods derived by variational means. *Mathematics of computation*, 24(109):23–26, 1970.
- Goldfarb, D., Ren, Y., and Bahamou, A. Practical quasi-newton methods for training deep neural networks. *arXiv preprint arXiv:2006.08877*, 2020.
- Gower, R., Goldfarb, D., and Richtárik, P. Stochastic block bfgs: Squeezing more curvature out of data. In *International Conference on Machine Learning*, pp. 1869–1878, 2016.
- Grosse, R. and Martens, J. A kronecker-factored approximate fisher matrix for convolution layers. In *International Conference on Machine Learning*, pp. 573–582, 2016.
- Gupta, V., Koren, T., and Singer, Y. Shampoo: Preconditioned stochastic tensor optimization. In Dy, J. and Krause, A. (eds.), *Proceedings of the 35th International Conference on Machine Learning*, volume 80 of *Proceedings of Machine Learning Research*, pp. 1842–1850. PMLR, 2018.
- Heskes, T. On ”natural” learning and pruning in multilayered perceptrons. *Neural Computation*, 12, 01 2000. doi: 10.1162/089976600300015637.
- Hinton, G., Srivastava, N., and Swersky, K. Neural networks for machine learning lecture 6a overview of mini-batch gradient descent. *Cited on*, 14(8), 2012.
- Kingma, D. and Ba, J. Adam: A method for stochastic optimization. *International Conference on Learning Representations*, 2014.
- Krizhevsky, A., Hinton, G., et al. Learning multiple layers of features from tiny images. 2009.
- Krizhevsky, A., Sutskever, I., and Hinton, G. E. Imagenet classification with deep convolutional neural networks. In Pereira, F., Burges, C. J. C., Bottou, L., and Weinberger, K. Q. (eds.), *Advances in Neural Information Processing Systems*, volume 25, pp. 1097–1105. Curran Associates, Inc., 2012. URL <https://proceedings.neurips.cc/paper/2012/file/c399862d3b9d6b76c8436e924a68c45b-Paper.pdf>.
- Liu, D. C. and Nocedal, J. On the limited memory bfgs method for large scale optimization. *Mathematical programming*, 45(1-3):503–528, 1989.
- Martens, J. Deep learning via hessian-free optimization. In *ICML*, volume 27, pp. 735–742, 2010.
- Martens, J. and Grosse, R. Optimizing neural networks with kronecker-factored approximate curvature. In *International conference on machine learning*, pp. 2408–2417, 2015.
- Povey, D., Zhang, X., and Khudanpur, S. Parallel training of dnns with natural gradient and parameter averaging. *arXiv preprint arXiv:1410.7455*, 2014.
- Ren, Y. and Goldfarb, D. Efficient subsampled gauss-newton and natural gradient methods for training neural networks. *arXiv preprint arXiv:1906.02353*, 2019.
- Robbins, H. and Monro, S. A stochastic approximation method. *The annals of mathematical statistics*, pp. 400–407, 1951.
- Schneider, F., Balles, L., and Hennig, P. DeepOBS: A deep learning optimizer benchmark suite. In *International Conference on Learning Representations*,

2019. URL <https://openreview.net/forum?id=rJg6sssC5Y7>.

Shanno, D. F. Conditioning of quasi-newton methods for function minimization. *Mathematics of computation*, 24 (111):647–656, 1970.

Simonyan, K. and Zisserman, A. Very deep convolutional networks for large-scale image recognition. *arXiv preprint arXiv:1409.1556*, 2014.

Springenberg, J. T., Dosovitskiy, A., Brox, T., and Riedmiller, M. Striving for simplicity: The all convolutional net. *arXiv preprint arXiv:1412.6806*, 2014.

Vinyals, O. and Povey, D. Krylov subspace descent for deep learning. In *Artificial Intelligence and Statistics*, pp. 1261–1268, 2012.

Wang, X., Ma, S., Goldfarb, D., and Liu, W. Stochastic quasi-newton methods for nonconvex stochastic optimization. *SIAM Journal on Optimization*, 27(2):927–956, 2017.

Xu, P., Roosta, F., and Mahoney, M. W. Newton-type methods for non-convex optimization under inexact hessian information. *Mathematical Programming*, pp. 1–36, 2019.

## A. Proof of Convergence of Algorithm KF-BFGS(L)-CNN and Associated Lemmas

Algorithm 3 gives the variant of KF-BFGS(L)-CNN that is used in the convergence proof.

**Algorithm 3** KF-BFGS(L)-CNN with  $D_{P(I)}D_{LM}$  and exact inversion of  $A$

**Require:** Given learning rates  $\{\alpha_k\}$ , damping values  $\lambda_A$  and  $\lambda_G$ , batch sizes  $\{m_k\}$ ,  $0 < \mu_1 < 1$ ,  $0 < \beta < 1$

- 1:  $A_l = \mathbb{E}_n [\sum_{t \in \mathcal{T}} \mathbf{a}_t^l(n) \mathbf{a}_t^l(n)^\top]$ ,  $H_A^l = (A_l + \lambda_A I_A)^{-1}$ ,  $H_G^l = I$ ,  $\mathbf{s}_G^l = \mathbf{y}_G^l = 0$  ( $l = 1, \dots, L$ )  
{Initialization}
- 2: **for**  $k = 1, 2, \dots$  **do**
- 3:   Sample mini-batch  $M_k$  of size  $m_k$
- 4:   Perform a forward-backward pass over  $M_k$  to compute stochastic gradient  $\widetilde{D}\mathbf{W}_l$  ( $l = 1, \dots, L$ )
- 5:   **for**  $l = 1, \dots, L$  **do**
- 6:      $W_l = W_l - \alpha_k H_G^l \widetilde{D}\mathbf{W}_l H_A^l$  { $H_G^l$  is initialized as an identity matrix in L-BFGS}
- 7:   **end for**
- 8:   Perform another forward-backward pass over  $M_k$  to compute  $\widetilde{\mathbf{h}}_l^+$  and  $\widetilde{D}\mathbf{h}_l^+$  ( $l = 1, \dots, L$ )
- 9:   **for**  $l = 1, \dots, L$  **do**
- 10:     {Compute  $H_A^l$ }
- 11:     Compute  $\hat{A}_l = \sum_t \widetilde{A}_{l,t}^l$ ,  $H_A^l = (\hat{A}_l + \lambda_A I)^{-1}$
- 12:     {Update  $H_G^l$  by damped L-BFGS}
- 13:      $\mathbf{s}_G^l = \beta \mathbf{s}_G^l + (1 - \beta) (\widetilde{\mathbf{h}}_l^+ - \widetilde{\mathbf{h}}_l)$ ,  $\mathbf{y}_G^l = \beta \mathbf{y}_G^l + (1 - \beta) (\widetilde{D}\mathbf{h}_l^+ - \widetilde{D}\mathbf{h}_l)$ .
- 14:      $(\widetilde{\mathbf{s}}_G^l, \widetilde{\mathbf{y}}_G^l) = D_{P(I)}D_{LM}(\mathbf{s}_G^l, \mathbf{y}_G^l)$  with  $H = H_G^l$ ,  $\mu_1 = \mu_1$ ,  $\mu_2 = \lambda_G$  {See Algorithm 4}
- 15:     Use L-BFGS with  $(\widetilde{\mathbf{s}}_G^l, \widetilde{\mathbf{y}}_G^l)$  to update  $H_G^l$
- 16:   **end for**
- 17: **end for**

**Algorithm 4**  $D_{P(I)}D_{LM}$

- 1: **Input:**  $\mathbf{s}, \mathbf{y}$ ; **Output:**  $\widetilde{\mathbf{s}}, \widetilde{\mathbf{y}}$ ; **Given:**  $0 < \mu_1 < 1, \mu_2 > 0$
- 2: **if**  $\mathbf{s}^\top \mathbf{y} < \mu_1 \mathbf{y}^\top \mathbf{y}$  **then**
- 3:    $\theta_1 = \frac{(1-\mu_1)\mathbf{y}^\top \mathbf{y}}{\mathbf{y}^\top \mathbf{y} - \mathbf{s}^\top \mathbf{y}}$
- 4: **else**
- 5:    $\theta_1 = 1$
- 6: **end if**
- 7:  $\widetilde{\mathbf{s}} = \theta_1 \mathbf{s} + (1 - \theta_1) \mathbf{y}$  {Powell's damping with  $H = I$ }
- 8:  $\widetilde{\mathbf{y}} = \mathbf{y} + \mu_2 \widetilde{\mathbf{s}}$  {Levenberg-Marquardt damping on  $H^{-1}$ }
- 9: **return:**  $\widetilde{\mathbf{s}}, \widetilde{\mathbf{y}}$

### A.1. Relevant Proofs for Theorem 1

#### A.1.1. PROOF OF LEMMA 1

*Proof.* First, similar to Powell's damping on  $H$ , we can show that  $\widetilde{\mathbf{s}}^\top \mathbf{y} \geq \mu_1 \mathbf{y}^\top \mathbf{y} \geq 0$ . Hence,  $\widetilde{\mathbf{s}}^\top \widetilde{\mathbf{y}} = \widetilde{\mathbf{s}}^\top \mathbf{y} + \mu_2 \widetilde{\mathbf{s}}^\top \widetilde{\mathbf{s}} \geq \mu_2 \widetilde{\mathbf{s}}^\top \widetilde{\mathbf{s}}$ .

To see the second inequality, by using that  $\widetilde{\mathbf{s}}^\top \widetilde{\mathbf{y}} \geq \widetilde{\mathbf{s}}^\top \mathbf{y}$  it follows that

$$\begin{aligned} \widetilde{\mathbf{y}}^\top \widetilde{\mathbf{y}} &= \mathbf{y}^\top \mathbf{y} + 2\mu_2 \widetilde{\mathbf{s}}^\top \mathbf{y} + \mu_2^2 \widetilde{\mathbf{s}}^\top \widetilde{\mathbf{s}} \\ &= \mathbf{y}^\top \mathbf{y} + 2\mu_2 \widetilde{\mathbf{s}}^\top \mathbf{y} + \mu_2 (\widetilde{\mathbf{s}}^\top \widetilde{\mathbf{y}} - \widetilde{\mathbf{s}}^\top \mathbf{y}) \\ &= \mathbf{y}^\top \mathbf{y} + \mu_2 \widetilde{\mathbf{s}}^\top \mathbf{y} + \mu_2 \widetilde{\mathbf{s}}^\top \widetilde{\mathbf{y}} \\ &\leq \mathbf{y}^\top \mathbf{y} + 2\mu_2 \widetilde{\mathbf{s}}^\top \mathbf{y} \\ &\leq \left(\frac{1}{\mu_1} + 2\mu_2\right) \widetilde{\mathbf{s}}^\top \widetilde{\mathbf{y}}. \end{aligned}$$

□

#### A.1.2. PROOF OF LEMMA 2

*Proof.* Corresponding to the BFGS update (9) of  $H$ , the update of  $B$  is

$$B^+ = B - \frac{B\mathbf{s}\mathbf{s}^\top B}{\mathbf{s}^\top B\mathbf{s}} + \rho\mathbf{y}\mathbf{y}^\top.$$

Hence,

$$\begin{aligned} \|B^+\| &\leq \|B - \frac{B\mathbf{s}\mathbf{s}^\top B}{\mathbf{s}^\top B\mathbf{s}}\| + \|\rho\mathbf{y}\mathbf{y}^\top\| \\ &\leq \|B\| + \frac{\mathbf{y}^\top \mathbf{y}}{\mathbf{s}^\top \mathbf{y}} \leq \|B\| + \frac{1}{\mu_3}. \end{aligned}$$

Also, using the fact that for the spectral norm  $\|\cdot\|$ ,  $\|I - \rho\mathbf{s}\mathbf{y}^\top\| = \|I - \rho\mathbf{y}\mathbf{s}^\top\|$ , we have that

$$\begin{aligned} \|H^+\| &\leq \|H\| \|I - \rho\mathbf{s}\mathbf{y}^\top\|^2 + \left\| \frac{\mathbf{s}\mathbf{s}^\top}{\mathbf{s}^\top \mathbf{y}} \right\| \\ &\leq \|H\| \left( \|I\| + \frac{\|\mathbf{s}\| \|\mathbf{y}\|}{\mathbf{s}^\top \mathbf{y}} \right)^2 + \frac{\mathbf{s}^\top \mathbf{s}}{\mathbf{s}^\top \mathbf{y}} \\ &\leq \left(1 + \frac{1}{\sqrt{\mu_2}} \frac{1}{\sqrt{\mu_3}}\right)^2 \|H\| + \frac{1}{\mu_2}. \end{aligned}$$

□

#### A.1.3. PROOF OF LEMMA 3

*Proof.* To simplify notation, we omit the subscript  $G$ , superscript  $l$  and the iteration index  $k$  in the proof. Hence, our goal is to prove  $\kappa_G I \preceq H = H_G^l(k) \preceq \bar{\kappa}_G I$ , for any  $l$  and  $k$ . Let  $(\mathbf{s}_i, \mathbf{y}_i)$  ( $i = 1, \dots, p$ ) denote the pairs used in an L-BFGS computation of  $H$ .

Given an initial estimate  $H_0 = B_0^{-1} = I$  of  $(G_l(\theta_k))^{-1}$ , the L-BFGS method updates  $H_i$  recursively as

$$H_i = (I - \rho_i \mathbf{s}_i \mathbf{y}_i^\top) H_{i-1} (I - \rho_i \mathbf{y}_i \mathbf{s}_i^\top) + \rho_i \mathbf{s}_i \mathbf{s}_i^\top, \quad (14)$$

where  $\rho_i = (\mathbf{s}_i^\top \mathbf{y}_i)^{-1}$ ,  $i = 1, \dots, p$ , and equivalently,

$$B_i = B_{i-1} - \frac{B_{i-1} \mathbf{s}_i \mathbf{s}_i^\top B_{i-1}}{\mathbf{s}_i^\top B_{i-1} \mathbf{s}_i} + \rho_i \mathbf{y}_i \mathbf{y}_i^\top, \quad i = 1, \dots, p,$$

where  $B_i = H_i^{-1}$ . Since we use  $D_{P(I)} D_{LM}$ , by Lemma 1, we have that  $\frac{\mathbf{s}_i^\top \mathbf{s}_i}{\mathbf{s}_i^\top \mathbf{y}_i} \leq \frac{1}{\mu_2}$  and  $\frac{\mathbf{y}_i^\top \mathbf{y}_i}{\mathbf{s}_i^\top \mathbf{y}_i} \leq \frac{1}{\mu_3}$ .

Hence, by Lemma 2, we have that  $\|B_i\| \leq \|B_{i-1}\| + \frac{1}{\mu_3}$ . Hence,  $\|B\| = \|B_p\| \leq \|B_0\| + \frac{p}{\mu_3} = 1 + \frac{p}{\mu_3}$ . Thus,  $B \preceq \left(1 + \frac{p}{\mu_3}\right) I$ , and  $H \succeq \left(1 + \frac{p}{\mu_3}\right)^{-1} I \equiv \underline{\kappa}_G I$ .

On the other hand, by Lemma 2, we have that  $\|H_i\| \leq \left(1 + \frac{1}{\sqrt{\mu_2 \mu_3}}\right)^2 \|H_{i-1}\| + \frac{1}{\mu_2}$ . Hence, from the fact that  $H_0 = I$ , and induction, we have that  $\|H\| \leq \hat{\mu}^p + \frac{\hat{\mu}^p - 1}{\hat{\mu} - 1} \frac{1}{\mu_2} \equiv \bar{\kappa}_G$ , where  $\hat{\mu} = \left(1 + \frac{1}{\sqrt{\mu_2 \mu_3}}\right)^2$ .  $\square$

#### A.1.4. PROOF OF LEMMA 4

*Proof.* First, because  $\hat{A}_l$  is the averaged value across the mini-batch, it suffices to show that for any data-point  $n$ ,  $\sum_t A_{t,t}^l(n) \preceq (J|\Delta|\varphi^2 + 1)|\mathcal{T}|I$ .

By AS. 3,  $\|\mathbf{a}_t(n)\|^2 = \sum_{j,\delta} a_{j,t+\delta}(n)^2 + 1 \leq J|\Delta|\varphi^2 + 1$ . Hence, for any vector  $\mathbf{x}$ ,

$$\begin{aligned} \mathbf{x}^\top A_{t,t}^l(n) \mathbf{x} &= \mathbf{x}^\top (\mathbf{a}_t(n) \mathbf{a}_t(n)^\top) \mathbf{x} = (\mathbf{a}_t(n)^\top \mathbf{x})^2 \\ &\leq \|\mathbf{a}_t(n)\|^2 \|\mathbf{x}\|^2 \leq (J|\Delta|\varphi^2 + 1) \|\mathbf{x}\|^2. \end{aligned}$$

Hence,  $A_{t,t}^l(n) \preceq (J|\Delta|\varphi^2 + 1)I$  and  $\sum_t A_{t,t}^l(n) \preceq (J|\Delta|\varphi^2 + 1)|\mathcal{T}|I$ , proving part (i).

Note that  $\hat{A}_l + \lambda_A I \succeq \lambda_A I$  because  $\hat{A}_l$  is PSD. On the other hand,  $\hat{A}_l + \lambda_A I \preceq ((J|\Delta|\varphi^2 + 1)|\mathcal{T}| + \lambda_A)I$ . Hence,

$$\begin{aligned} ((J|\Delta|\varphi^2 + 1)|\mathcal{T}| + \lambda_A)^{-1} I &\preceq H_A^l \\ &= (\hat{A}_l + \lambda_A I)^{-1} \preceq \lambda_A^{-1} I. \end{aligned} \quad (15)$$

By (15) and Lemma 3, we have that  $\underline{\kappa} I \preceq H_A^l \otimes H_G^l = H_l \preceq \bar{\kappa} I$  where  $\underline{\kappa} = ((J|\Delta|\varphi^2 + 1)|\mathcal{T}| + \lambda_A)^{-1} \underline{\kappa}_G$ ,  $\bar{\kappa} = \lambda_A^{-1} \bar{\kappa}_G$ . Finally,  $\underline{\kappa} I \preceq H = \text{diag}\{H_1, \dots, H_L\} \preceq \bar{\kappa} I$ .  $\square$

#### A.1.5. PROOF OF THEOREM 1

*Proof.* First, Algorithm 3 falls in the general framework of the Stochastic Quasi-Newton (SQN) method (Algorithm

2.1) in (Wang et al., 2017). Second, by Lemma 4, Assumption AS.3 in (Wang et al., 2017) is satisfied. Also, by the way  $H_A$  and  $H_G$  are updated, AS.4 in (Wang et al., 2017) is satisfied. Hence, since Assumptions AS.1 and AS.2 are identical to the other two assumptions made in (Wang et al., 2017), we are able to apply Theorem 2.8 in that paper to Algorithm 3 in this Section.  $\square$

## B. Implementation Details

### B.1. Specification on Algorithms

---

#### Algorithm 5 KFAC

---

**Require:** Given learning rate  $\alpha$ , damping value  $\lambda$ , batch size  $m$ , inversion frequency  $T$

- 1:  $\widehat{\mathcal{D}W}_l = 0$ ,  $\Omega_l = \mathbb{E}_n [\sum_{t \in \mathcal{T}} \mathbf{a}_t^l(n) \mathbf{a}_t^l(n)^\top]$ ,  $\Gamma_l = \mathbb{E}_n [\widehat{\mathcal{D}h}^l(n) (\widehat{\mathcal{D}h}^l(n))^\top]$  ( $l = 1, \dots, L$ ) {Initialization}
  - 2: **for**  $k = 1, 2, \dots$  **do**
  - 3:   Sample mini-batch  $M_k$  of size  $m$
  - 4:   Perform a forward-backward pass over the current mini-batch  $M_k$  to compute  $\widehat{\mathcal{D}W}_l$  for  $l = 1, \dots, L$
  - 5:   **for**  $l = 1, 2, \dots, L$  **do**
  - 6:      $\widehat{\mathcal{D}W}_l = \beta \widehat{\mathcal{D}W}_l + (1 - \beta) \widehat{\mathcal{D}W}_l$
  - 7:      $p_l = H_\Gamma^l \widehat{\mathcal{D}W}_l H_\Omega^l$
  - 8:      $W_l = W_l - \alpha \cdot p_l$ .
  - 9:   **end for**
  - 10:   Perform another pass over  $M_k$  with  $y$  sampled from the predictive distribution to compute  $\widehat{\mathcal{D}h}_t^l$  for  $l = 1, \dots, L$
  - 11:   **for**  $l = 1, 2, \dots, L$  **do**
  - 12:     Update  $\Omega_l = \beta \cdot \Omega_l + (1 - \beta) \cdot \sum_{t \in \mathcal{T}} \widetilde{\mathbf{a}_t^l} (\widetilde{\mathbf{a}_t^l})^\top$ ,  
 $\Gamma_l = \beta \cdot \Gamma_l + (1 - \beta) \cdot \widetilde{\mathcal{D}h}_t^l (\widetilde{\mathcal{D}h}_t^l)^\top$
  - 13:     **if**  $i \equiv 0 \pmod{T}$  **then**
  - 14:       Recompute  $H_\Omega^l = (\Omega_l + \sqrt{\lambda} I)^{-1}$ ,  $H_\Gamma^l = (\Gamma_l + \sqrt{\lambda} I)^{-1}$
  - 15:     **end if**
  - 16:   **end for**
  - 17: **end for**
- 

We describe the version of KFAC that we implemented in Algorithm 5. Note that  $\Omega_l$  in KFAC is the same as  $A_l$  is our paper. Similar to the pseudo-code of KF-QN-CNN, we assume that all layers are convolutional.

Note that KFC-pre in (Grosse & Martens, 2016) differs from Algorithm 5 in the following ways:

- KFC-pre uses  $\pi_l$  to decide how to split  $\lambda$  into  $\lambda_\Omega$  and  $\lambda_\Gamma$
- KFC-pre uses clipping for the approximated natural

gradient direction  $p$

- KFC-pre uses momentum for  $p$
- KFC-pre uses parameter averaging on  $\theta$

Note that most of these techniques can also be applied to KF-QN-CNN. Since we are primarily interested in comparing different pre-conditioning matrices, we chose not to include such techniques in our implementation.

Also note that in Algorithm 5, a warm start computation of  $\Omega_l$  and  $\Gamma_l$  is included, i.e. initial estimates of  $\Omega_l$  and  $\Gamma_l$  are computed from the whole dataset before the first iteration. A similar warm start computation of  $A_l$  was also included in KF-QN-CNN. Since these warm start computations take no more than the time for one epoch, we did not include the times for warm starts in the figures.

Finally, Adam was implemented exactly as in (Kingma & Ba, 2014).

## B.2. More Details on the Experiments

The All-CNN-C model from (Springenberg et al., 2014) consists of 9 convolutional layers with either  $3 \times 3$  or  $1 \times 1$  filters and strides of 1 or 2. The VGG16 model refers to the "model D" in (Simonyan & Zisserman, 2014), which consists of 13 convolutional layers with  $3 \times 3$  filters, and 3 fully-connected layers.

The grid search ranges for Figures 1 and 2 are given below:

- KF-QN-CNN and KFAC:
  - Learning rate  $\alpha \in \{0.1, 0.3, 1, 3, 10, 30, 100, 300, 1000\}$
  - Damping  $\lambda \in \{0.1, 0.3, 1, 3, 10, 30, 100\}$
- Adam:
  - Learning rate  $\alpha \in \{1e-5, 3e-5, 1e-4, 3e-4, 1e-3, 3e-3, 0.01, 0.03, 0.1\}$
  - Damping  $\epsilon \in \{1e-12, 1e-8, 1e-4, 0.01, 0.1\}$
- SGD-m: learning rate  $\alpha \in \{1e-3, 3e-3, 0.01, 0.03, 0.1, 0.3, 1\}$

Table 3 lists the best HP values found by grid search for the five methods tested. Note that sometimes second-order methods found that the best damping value to be the largest value of 100 in our grid search. We explored increasing damping value beyond 100, but found that the performance barely changed, as long as a good learning rate was chosen.

Besides the tuned HPs, we set the following HPs to fixed default values:

- $L_2$  regularization: 0.0005 (note that this was not included in the loss value, but was added when computing gradient)
- Decay parameters  $\beta = 0.9$  for KF-QN-CNN (Algorithm 2), KFAC (Algorithm 5), SGD-m (for updating the momentum of gradient), and  $\beta_1 = \beta_2 = 0.9$  in Adam (Kingma & Ba, 2014).
- For KF-BFGS-CNN and KF-BFGS(L)-CNN,  $\mu_1 = 0.2$  in  $D_P D_{LM}$ . The algorithms are not sensitive to the value of  $\mu_1$ , hence it was set to a default value.
- For KF-BFGS(L)-CNN, the number of (s, y) pairs stored for L-BFGS was set to a default value of  $p = 100$ .
- For KFAC, the inversion frequency was set to  $T = 20$ , as in (Martens & Grosse, 2015).

## B.3. Stability of KF-QN-CNN

In Fig 3, we plot the performance of KF-BFGS-CNN on the same four problems that were used to obtain the results plotted in Figures 1 and 2, with damping values of  $\lambda \in \{0.3, 1, 3, 10, 30, 100\}$  and their corresponding best learning rates. SGD with momentum is also plotted as a baseline. We can see that, in our experiments, KF-BFGS-CNN is not very sensitive to the choice of the damping value when combined with the best learning rate for that choice.

## B.4. Overfitting Problem on (CIFAR100, VGG16)

In order to double check the overfitting issue that occurred on CIFAR100 with the VGG16 model, we chose the best HP values based on the classification accuracy on the testing set rather than on the training loss and plotted Fig 4. With the new set of HP values, the first-order methods no longer overfit the training set. The comparison between the algorithms that we tested in this case is similar to that of Fig 1 b).



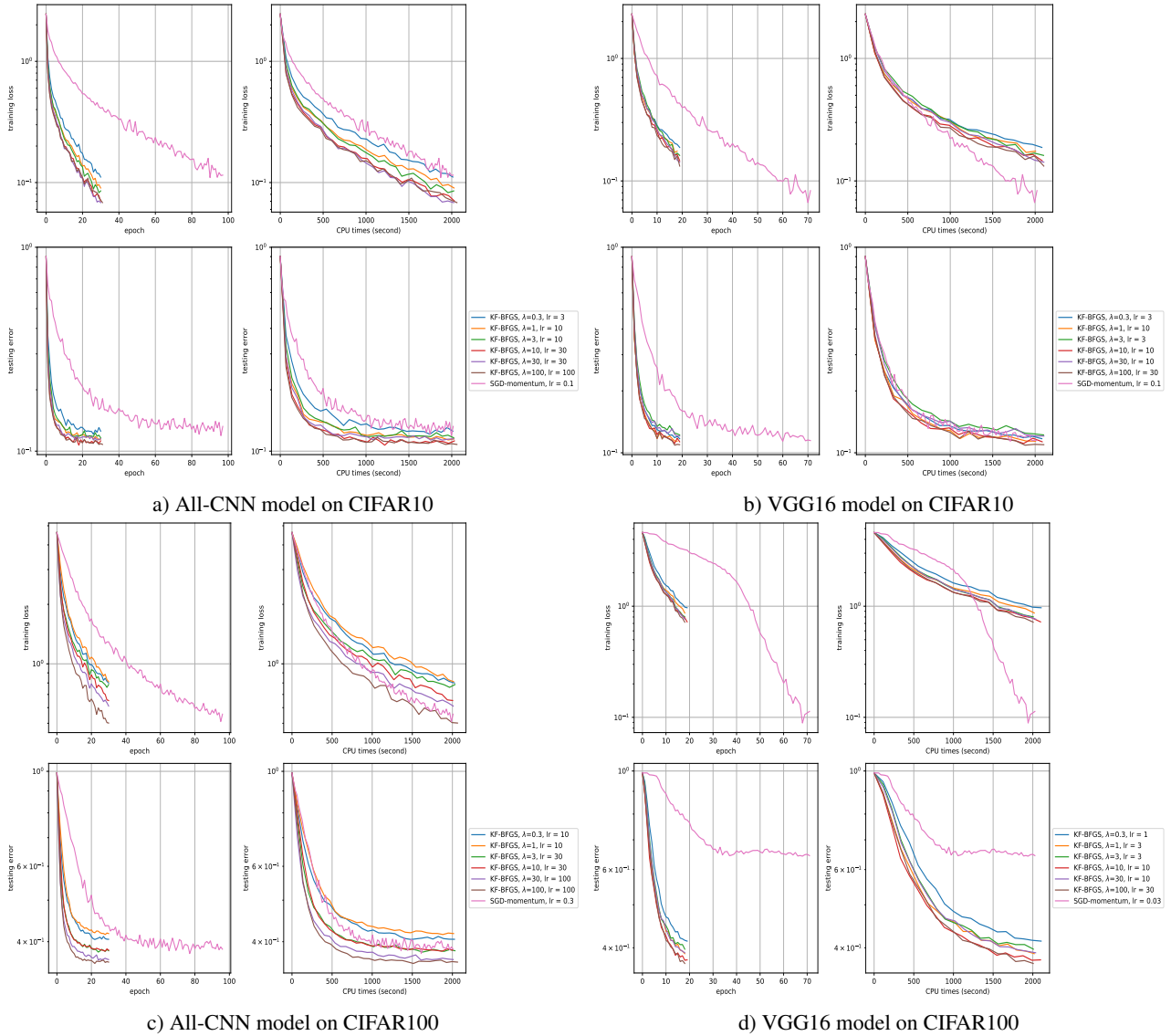


Figure 3. Demonstration of the stability of KF-BFGS-CNN with different HP values (KF-BFGS-CNN is denoted as KF-BFGS in the legend)

Table 3. (Learning rate, damping) values for Figures 1 and 2

	KF-BFGS-CNN	KF-BFGS(L)-CNN	KFAC	Adam	SGD-m
All-CNN-C on CIFAR10	(30, 30)	(30, 30)	(100, 30)	(1e-4, 1e-4)	(0.1, -)
VGG16 on CIFAR10	(30, 100)	(3, 3)	(100, 100)	(0.01, 0.1)	(0.1, -)
All-CNN-C on CIFAR100	(100, 100)	(100, 100)	(1000, 100)	(1e-4, 1e-8)	(0.3, -)
VGG16 on CIFAR100	(30, 100)	(10, 100)	(1, 0.3)	(1e-3, 0.01)	(0.03, -)

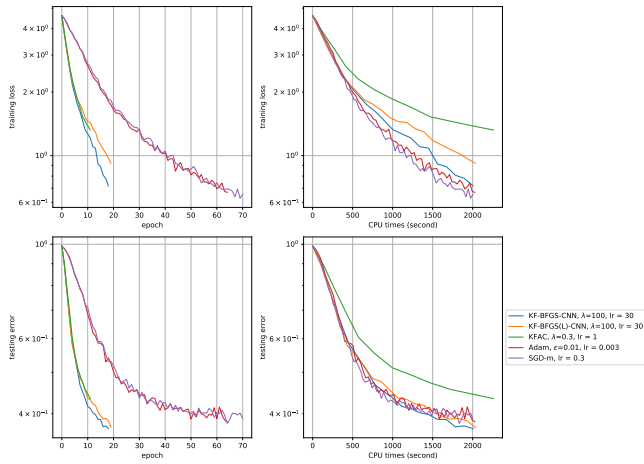


Figure 4. Comparison between algorithms on CIFAR100 with the VGG16 model, where HP values were chosen based on testing performance